Chapter 9

Ionic Polymer Metal Composite Transducer and Self-Sensing Ability

Doan Ngoc Chi Nam and Ahn Kyoung Kwan

Additional information is available at the end of the chapter

http://dx.doi.org/10.5772/51310

1. Introduction

During the recent decade, ionic polymer metal composite (IPMC), as a smart material, is gaining great importance in the use for both sensors and actuators. An ion polymer metal composite (IPMC) is an Electro-Active Polymer (EAP) that bends in response to a small applied electrical field as a result of mobility of cations in the polymer network [1] and vice versa. A typical IPMC sheet is constructed with a thin (200 μm) ionic polymer membrane like Nafion or Flemion and two metalic electrode layers (10 μm thick) outside such as platinum or gold. When a low voltage electrical field (1 – 5V) is applied, the transport of hydrated cations within the solvated IPMC and the associated electrostatic interactions lead to bending motions of the IPMC sheet. Thus, an IPMC can work as a small size actuator. Figure 1 illustrates the mechanism of the IPMC as actuator. On the other hand, when an IPMC is mechanically bent, it will generate a low voltage (order of milivolts) between the two electrodes. The generated voltage is due to the non-uniform concentration of ions in the IPMC membrane. Figure 2 illustrates the behavior of the IPMC as sensor.

Since firstly introduced, the IPMC has been applied in many research fields such as biomedical system, biomimetic robot, and MEMS devices. In these applications, the IPMC may give advantages thank to the low driven voltage, flexible operation, and simple actuating structure. Some applications using IPMC material have been a snake-like robot with IPMC actuator [7], a micro pump [8], a scale biped walking robot [9], an underwater micro robot [10], etc. Because of the increasing importance of IPMC in the smart material field, it is important to clearly understand the behavior inside the IPMC actuator.

Recently, it has been found that the IPMC possesses an attractive characteristic which is so called the "self – sensing" behavior. The self – sensing ability originates from the variation of surface resistance of the two electrode layers during operating period [11 – 12]. If one can capture these variations of surface resistance, the bending curvature can be figured out. The self – sensing ability has been one of the most interesting features of the IPMC transducer.

By employing self – sensing feature, the sensing problem will be easier for the field of biomedical devices, biomimetic and micro robots.

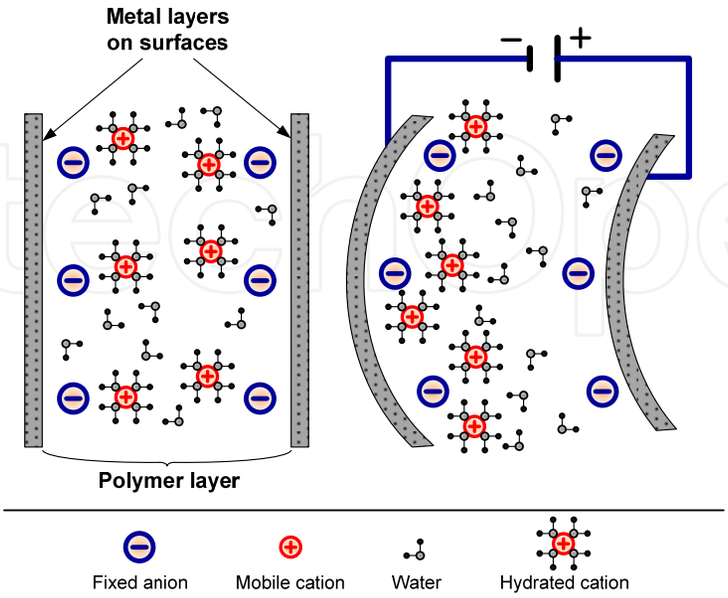

Figure 1. Operating principle of IPMC as actuator

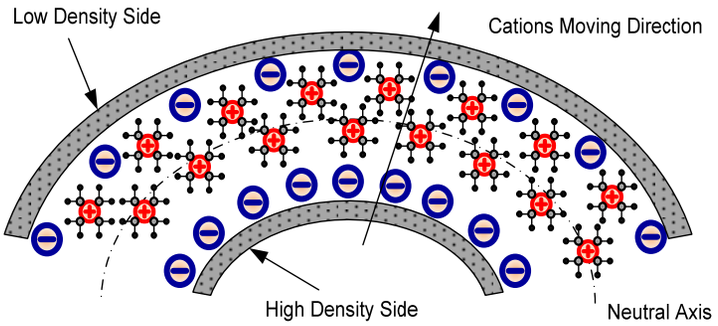

Figure 2. Fundamental of IPMC as a motion sensor

In order to investigate the behavior of IPMC and its self- sensing ability, this chapter will cover physical analysis on an IPMC actuator and its self – sensing model. Firstly, the mechanism inside the IPMC actuator under an applied input voltage signal is carried out. The analysis starts from the governing partial differential equation (PDE) for charge distribution in an IPMC, which was introduced firstly by Nasser et al. in [13] and then used in [14] and [15] for investigating the actuation and sensing response. The effect of distributed surface resistance is also considered to obtain accurate boundary conditions for the PDE. Solving the PDE in asymmetric boundary conditions, the charge density inside the IPMC is obtained. Consequently, the induced stress of the IPMC is obtained. Using this induced stress model, a visual simulation technique is proposed for investigating the actuation capabilities of IPMC actuator via ANSYS environment [18].

Next, the self – sensing ability of the IPMC actuator is analyzed. The self sensing technique is inspired by the variation of surface resistance along the IPMC. An equivalent circuit of

IPMC actuator is present and analyzed. Consequently, a simple technique to implement the self – sensing behavior of IPMC is carried out. In this technique, the variation of surface resistance along the IPMC is figured out using half clamped configuration. Four voltage feedback signals are then employed to estimate the bending behavior. Experimental results show that this technique has a strong ability to apply the self – sensing technique into real application, i.e. micro robot, biomimetic robot.

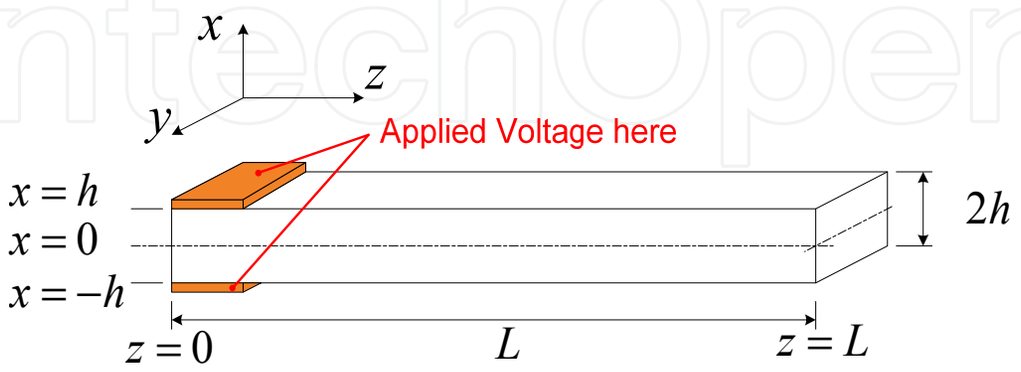

Figure 3. Geometric description of IPMC transducer

2. Electromechanical model of IPMC actuator

The electromechanical model developed for the Nafion based IPMC relies on field and continuity equations. Let D, E, ϕ, and ρ denote the electric displacement, the electric field, the electric potential, and the charge density, respectively, the field equations and continuity equation using in this analysis are as follows:

$$E = \frac{D}{\kappa_e} = -\nabla\phi \tag{1}$$

$$\nabla \cdot D = \rho = F\left(C^+ - C^-\right) \tag{2}$$

$$\nabla \cdot J = -\frac{\partial C^+}{\partial t} \tag{3}$$

where, κ_e is the effective dielectric constant of the polymer, F is Faraday's constant, J is the ion flux vector, and C^+ and C^- are the cation and anion concentrations, respectively. The ion flux is considered to be composed of three primary terms: the diffusion, migration and convection terms:

$$J = -d\left(\nabla C^+ + \frac{C^+F}{RT}\nabla\phi + \frac{C^+\Delta V}{RT}\nabla p\right) + C^+ v \tag{4}$$

where, d is the ionic diffusivity, R is the gas constant, T is the absolute temperature, p is the fluid pressure, v is the free solvent velocity field, and ΔV is the volumetric change.

Considering the geometric description of IPMC as in figure 3, since the thickness of an IPMC is much smaller than its length or width, the first assumption is claimed as: inside the polymer, D, E, and J are all restricted to the thickness direction (x-direction). This assumption enables to drop the boldface notation for these variables. Rewrite equation (2) as:

$$C^+ = \frac{1}{F}\rho + C^- \tag{5}$$

Because the anions are constrained to the polymer backbone, the concentration of anions inside the IPMC is considered to be spatially and temporally constant. Therefore, the cation gradient can be rewritten specifically in terms of the electric field E:

$$\nabla C^+ = \frac{\kappa_e}{F}\nabla^2 E \tag{6}$$

Employing a modified version of Darcy's Law [29], the free solvent velocity field can be calculated as:

$$v = k^{'}\left[C^- FE - \nabla p\right] \tag{7}$$

where $k^{'}$ represents the hydraulic permeability. The second assumption is that the convection term can be neglected: $v \to 0$. Then, equation (7) becomes:

$$\nabla p = C^- FE \tag{8}$$

By employing equations (5), (6) and (8), the original flux equation (4) can be rewritten as:

$$J = -d\left(\frac{\kappa_e}{F}\nabla^2 E - \frac{\left(1 - C^-\Delta V\right)}{RT}E\left(\kappa_e \nabla E - FC^-\right)\right) \tag{9}$$

By taking the gradient of (9) and employing (3), the nonlinear PDE in term of electrical field is obtained as:

$$-\frac{\kappa_e}{F}\frac{\partial\left(\nabla E\right)}{\partial t} = -d\left(\frac{\kappa_e}{F}\nabla^3 E - \frac{\kappa_e\left(1 - C^-\Delta V\right)}{RT}\left(\nabla^2 E.E + \left(\nabla E\right)^2\right) - \frac{FC^-\left(1 - C^-\Delta V\right)}{RT}\nabla E\right) \tag{10}$$

Consider the properties of the IPMC actuator as shown in table 1. It can be seen that the coefficient ratio of the linear term and the nonlinear term:

$$ratio = \frac{FC^-}{\kappa_e} \tag{11}$$

is around the order of 5×10^{10}. Hence, it can be concluded that:

$$\frac{\kappa_e\left(1-C^-\Delta V\right)}{RT}\left(\nabla^2 E.E+\left(\nabla E\right)^2\right)<<\frac{FC^-\left(1-C^-\Delta V\right)}{RT}\nabla E \tag{12}$$

Neglecting small nonlinear term, the PDE for the electric field can be obtained as:

$$\frac{\partial}{\partial x}\left[\frac{\partial\left(\kappa E\right)}{\partial t}-d\frac{\partial^2\left(\kappa E\right)}{\partial x^2}-\frac{F^2dC^-}{\kappa RT}\left(1-C^-\Delta V\right)\left(\kappa E\right)\right]=0 \tag{13}$$

or in the form of charge density ρ :

$$\frac{\partial\rho}{\partial t}-d\frac{\partial^2\left(\rho\right)}{\partial x^2}-\frac{F^2dC^-}{\kappa RT}\left(1-C^-\Delta V\right)\rho=0 \tag{14}$$

where, C^- is the anion concentration and κ is the effective dielectric constant of the polymer.

$F=96487\ {C}/{mol}$	$R=8.3143\ {J}/{mol\cdot K}$	$T=300K$	$w=0.02mm$
$h=100\,\mu m$	$d=1.030\times10^{-10}m^2/s$	$C^-=1200mol/m^3$	$\kappa=1.88\mu F/m$

Table 1. Parameters of IPMC charging model

The solutions of (13) and (14) are analyzed as follows:

It is noted that the IPMC transducer consists of two noble metallic layers outside as electrodes and one ion-exchange polymer membrane with fixed anions at both sides and movable cations. Because of the fixed anion layers, an applied step voltage will lead to an asymmetry in the ion redistribution [16 – 17].

Considering the steady state where $J=0$, the PDE (13) becomes:

$$\frac{\partial^2 E}{\partial x^2}-KE=0 \tag{15}$$

where:

$$K\triangleq\frac{F^2C^-}{\kappa RT}\left(1-C^-\Delta V\right) \tag{16}$$

Since fixed anions locate at both sides of the polymer membrane (see figure 1), the charge density in the anode boundary layer keeps a constant value, given by:

$$\rho_{(1)}=-C^-F \tag{17}$$

Whereas, in the remaining part, the charge density is given as:

$$\rho_{(2)}=\left(C^+-C^-\right)F \tag{18}$$

Thus, the charge density ρ, electric field E, and electric potential field ϕ in the anode boundary layer are then given by:

$$\begin{cases} \rho_{(1)}(x) = -C^{-}F \\ E_{(1)}(x) = \dfrac{1}{\kappa}\left(-C^{-}Fx + E_0\right) \qquad \text{for}\left(-h \le x \le -h+w\right) \\ \phi_{(1)}(x) = \dfrac{1}{\kappa}\left(\dfrac{C^{-}Fx^2}{2} - E_0 x\right) + A_0 \end{cases} \tag{19}$$

where, w is the thickness of the anode boundary layer, E_0, and A_0 are an integration constants. In the remaining region, solution of the ODE (5) can be obtained as:

$$\begin{cases} E_{(2)}(x) = C_1 \exp(\sqrt{K}x) + C_2 \exp(-\sqrt{K}x) \\ \phi_{(2)}(x) = \dfrac{1}{\sqrt{K}}\left(-C_1 \exp(\sqrt{K}x) + C_2 \exp(-\sqrt{K}x)\right) + C_3 \quad \text{for}\left(-h+w \le x \le h\right) \\ \rho_{(2)}(x) = \kappa\sqrt{K}\left(C_1 \exp(\sqrt{K}x) - C_2 \exp(-\sqrt{K}x)\right) \end{cases} \tag{20}$$

where, C_1, C_2, and C_3 are integration constants. Consequently, the function of charge density in steady state is obtained for an IPMC actuator under a step voltage input signal:

$$\rho^{*}(x) = \begin{cases} -C^{-}F & \text{for}\left(-h \le x \le -h+w\right) \\ \kappa\sqrt{K}\left(C_1 \exp(\sqrt{K}x) - C_2 \exp(-\sqrt{K}x)\right) & \text{for}\left(-h+w \le x \le h\right) \end{cases} \tag{21}$$

3. Effect of distributed surface resistance in an IPMC actuator

In order to find correct value for the charge density ρ, electric field E, and electric potential field ϕ, a sufficient set of boundary conditions must be considered. In this section, the effect of distributed surface resistance is investigated to serve as a boundary condition for solving the distribution of charge density, electric field, and electric potential along the z axis. Since the chemical reduction of salt is typically used to build the electrode layers, the surfaces of an IPMC typically consist of aggregated nano particles of noble metal. Thus, the affect of surface resistance is non-negligible in the behavior of IPMC during sensing and actuating process.

Considering the effect of distributed surface resistance, the equivalent circuit of the IPMC is shown as in figure 4. Let the electrode resistance per unit length be r_1 in z direction and r_2 in x direction. As shown in figure 4, $i_p(z,t)$ is the distributed current per unit length going through the polymer due to the ion movement, $i_k(z,t)$ represents the leaking current per unit length, and $i_s(z,t)$ is the surface current on the electrodes. R_{dc} denotes the leakage resistance per unit length. The surface current $i_s(0,t)$ at $z=0$ is the total actuation current. The following equations hold for the impedance model:

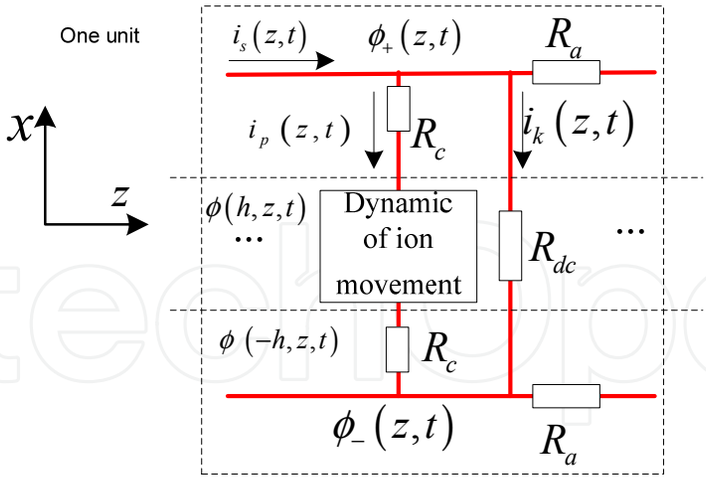

Figure 4. Equivalent circuit of IPMC in a unit length

$$\frac{\partial \phi_{\pm}(z,t)}{\partial z} = \mp R_a i_s(z,t) \tag{22}$$

$$\frac{\partial i_s(z,t)}{\partial z} = -\left(i_p(z,t) + i_s(z,t)\right) \tag{23}$$

Under the effect of distributed surface resistance, the first two boundary conditions for the PDE are:

$$\frac{\partial \phi(h,z,t)}{\partial z} = \int_0^z R_a i_s(\tau,t)d\tau - R_c i_p(z,t) \tag{24}$$

$$\frac{\partial \phi(-h,z,t)}{\partial z} = \phi_0 - \int_0^z R_a i_s(\tau,t)d\tau - R_c i_p(z,t) \tag{25}$$

Other boundary conditions are described as:

$$C^+(-h+\mathrm{w}) = 0 \tag{26}$$

$$E_{(1)}(-h+\mathrm{w}) = E_{(2)}(-h+\mathrm{w}) \tag{27}$$

$$\phi_{(1)}(-h+\mathrm{w}) = \phi_{(2)}(-h+\mathrm{w}) \tag{28}$$

These constraints are continuity, and the overall charge-balance conditions. By employing the above constraints, one can solve for E_0, A_0, C_1, C_2, and C_3 to obtain the distribution of charge density, electric field, and voltage potential along the z axis.

Approximately, the dynamic of charging model can be express as:

$$\rho(x,t)=\left(1-\exp\left(\frac{-t}{\tau}\right)\right)\rho^{*}(x),\quad \tau=\frac{\kappa RT}{dC^{-}F} \tag{29}$$

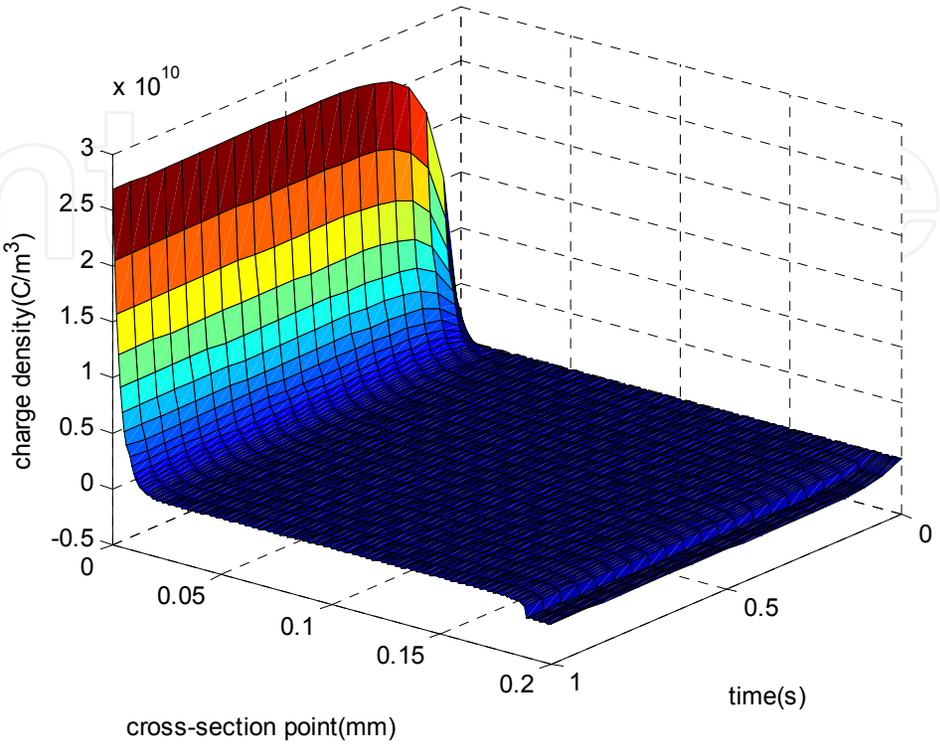

Figure 5. Simulation result for the charge density profile

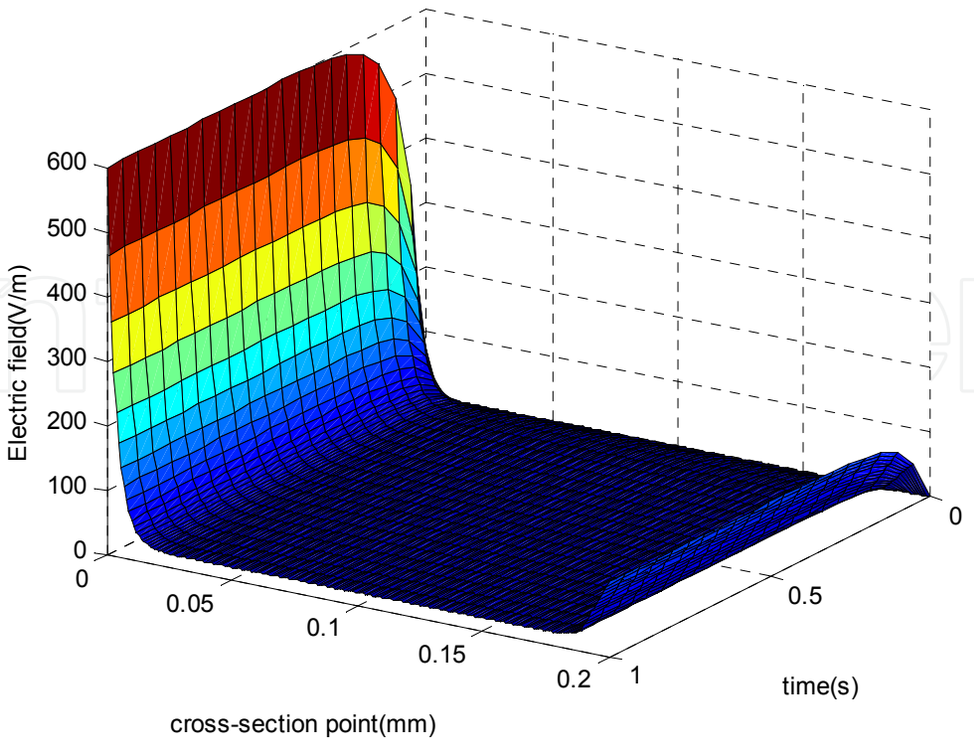

Figure 6. Simulation result for the distributed electric field

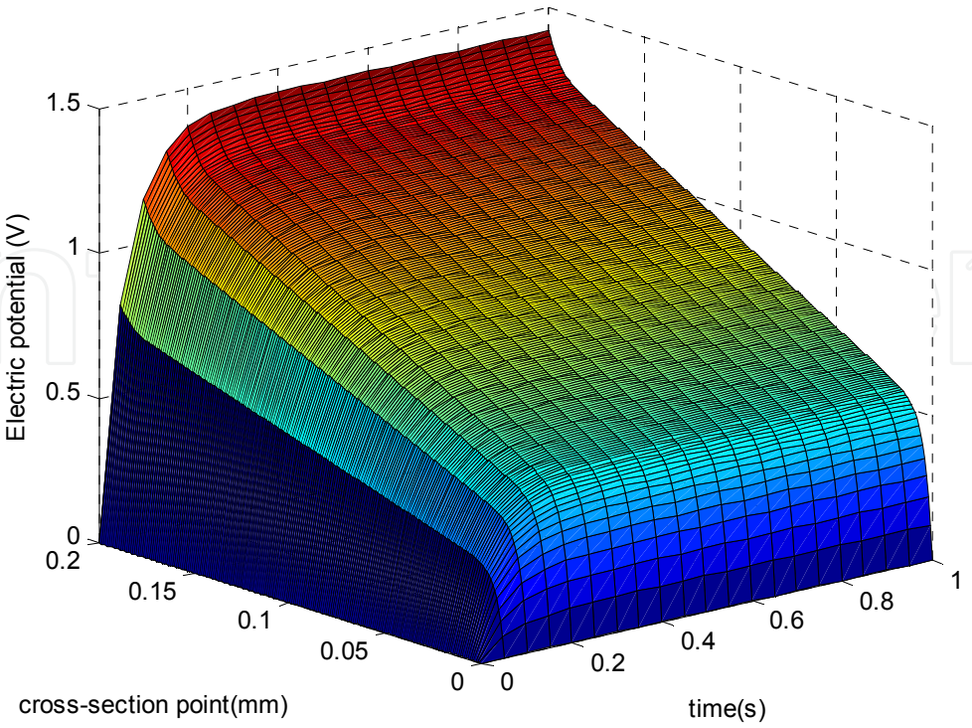

Figure 7. Simulation result for the distributed voltage potential

Here, τ is the natural time scale which characterizes relative speed of cation redistribution. Applying the above analysis, the charging behavior, the distributed electric field, and the distributed electric potential can be trivially obtained. Figure 5, figure 6, and figure 7 are the step response of the charge density, electric field, and electric potential when a 1.5V step input voltage signal is applied to the IPMC actuator.

4. Visual analysis of IPMC actuator

Since the charge distribution is obtained, the induced stress inside the IPMC actuator is available. The key assumption for analysis the electromechanical behavior inside the IPMC transducer is that the induced stress inside the IPMC σ is proportional to the electric charge density ρ :

$$\sigma(x,y,z,t)=\alpha_0\rho(x,y,z,t) \tag{30}$$

where, α_0 is the coupling constant to be determined by experiment. The internal stress σ produces the deformation of the IPMC actuator. Generally, the ideal linear beam theory is employed to analyze the bending behavior of a beam configured IPMC actuator. The bending moment is obtained by integration of induced stress along the x axis. However, this is a complicated work since the induced stress σ is not in simple form. Moreover, if the configuration of IPMC is complex (i.e. round shape, triangular shape), the above technique is unavailable.

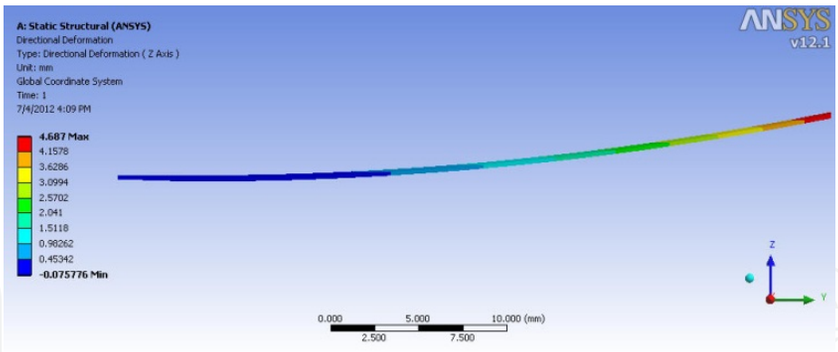

(a) Displacement of cantilever IPMC actuator (iso view)

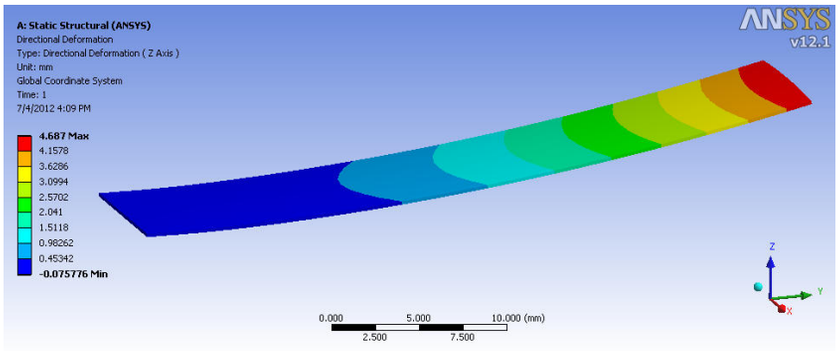

(b) Displacement of cantilever IPMC actuator (front view)

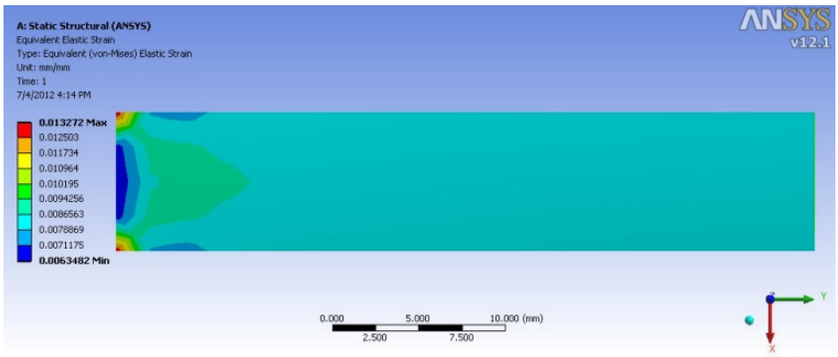

(c) Strain of cantilever IPMC actuator (top view)

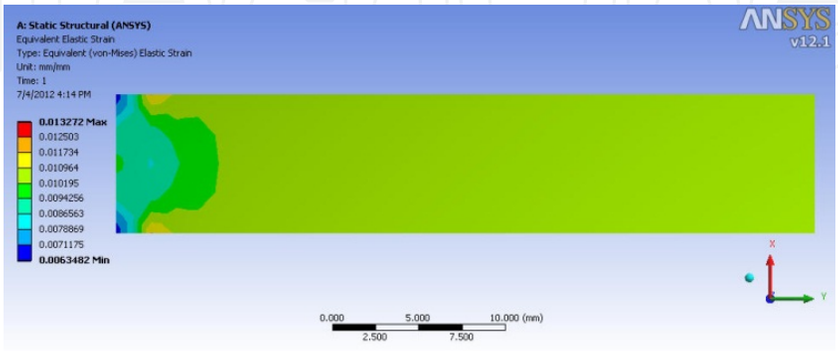

(d) Strain of cantilever IPMC actuator (bottom view)

Figure 8. Simulation of a cantilever IPMC actuator

For ease of analysis, this chapter proposes a novel visual simulation technique for the IPMC actuator using a commercial mechanical analysis tool, ANSYS 12.1 (2009) [18]. In this technique, a finite element model (FEM) is created to model an IPMC actuator. By using the command "INISTATE", the induced stress, obtained from equation (30), is added to the FEM as the deformation mechanism. Next, the constraints at the clamped edges of the IPMC actuator are considered as boundary conditions (fixed support to the clamped edges). Displacement constraints are employed as boundary conditions for neutral plane inside the IPMC actuator.

An example of visual simulation is shown as figure 8 for the cantilever IPMC actuator with a constant 3V input signal. The material properties of the IPMC actuator, employed for the FEM, are shown as in Table 2. A FEM with total 400 elements was created. As shown in figure 8a and figure 8b, the deformation of the IPMC can reach 4.69 mm at maximum under 3V input signal. Figure 8c and figure 8d show the internal strain ratio of the IPMC actuator under operation (maximum strain ratio is 0.013). Figure 9 shows the response of the IPMC beam under a step input voltage signal, and figure 10 shows the displacement versus input voltage graph at the steady state. Modeling results show that the visual simulation technique possesses a strong ability to be applied in analyzing operation of IPMC. It is obvious that the proposed visual simulation technique helps to analyze the behaviors of IPMC actuators more conveniently. In high input voltage signal range, the experimental displacements of IPMC are smaller than simulations. The reasons may be caused by the incompetence of the key assumption (see equation 30), the neglecting of nonlinear term in the PDE, or the variation of surface resistance along the z axis when the IPMC deforms.

	Elastic modulus (Pa)	Poisson's ratio	Size of IPMC actuator (mm)	Diaphragm radius (mm)	Thickness (mm)
Specification	5.71×10^{8}	0.487	$30\times6\times0.2$	5	0.2

Table 2. Material properties of IPMC diaphragm

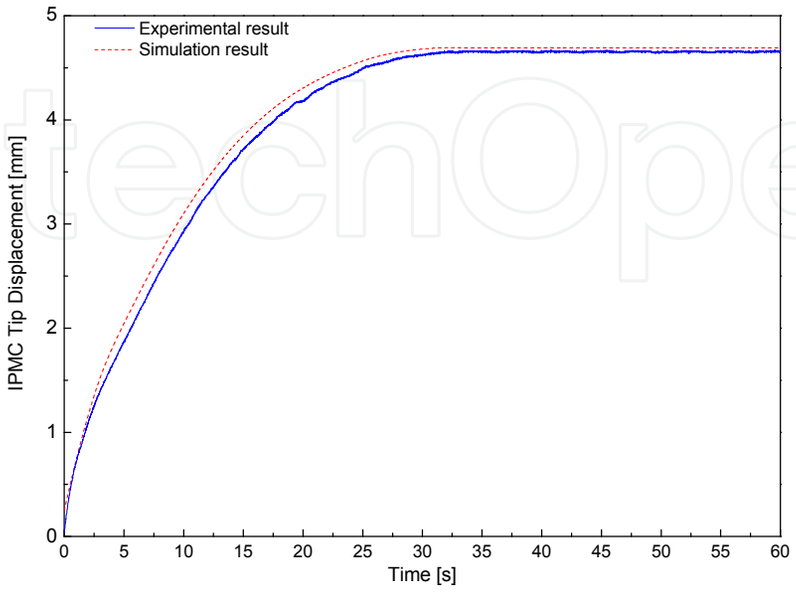

Figure 9. IPMC actuation with respect to a 3V step input signal

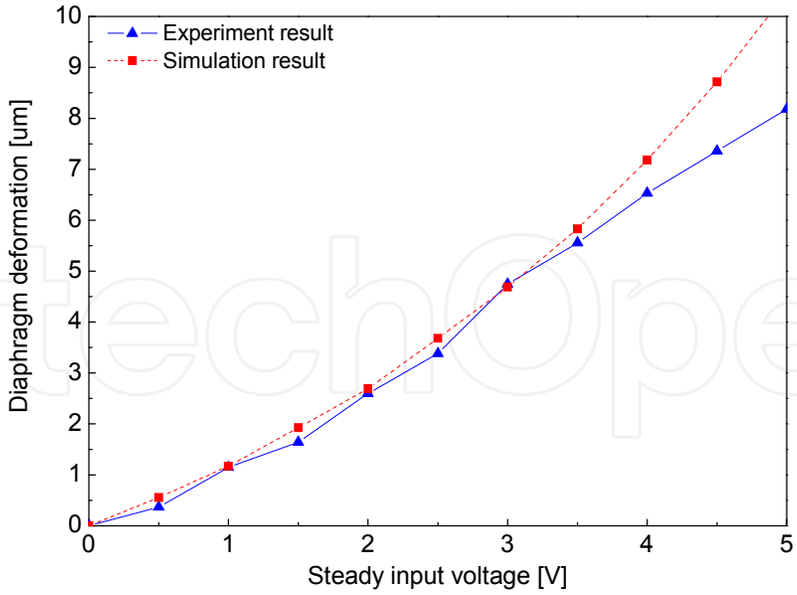

Figure 10. Displacement vs. input voltage

5. Variation of surface resistance and self sensing ability

5.1. Physical model of self sensing ability

During the bending operation, surface resistances of the two electrode layers may change due to the non – uniform material distribution between the two electrode layers as reported in [11 – 12]. During the deforming process, the surface resistance on the stretched side of IPMC increases corresponding to the reduction of conductive material density. Meanwhile, the surface resistance on the compressed side of IPMC decreases because the density of conductive material on the surface layer increases. In order to investigate the bending curvature - surface resistance correlation, a simple model of an IPMC sheet is derived out as in figure 11. Here, half of the IPMC sheet is fixed by a clamp while the other half sheet is free

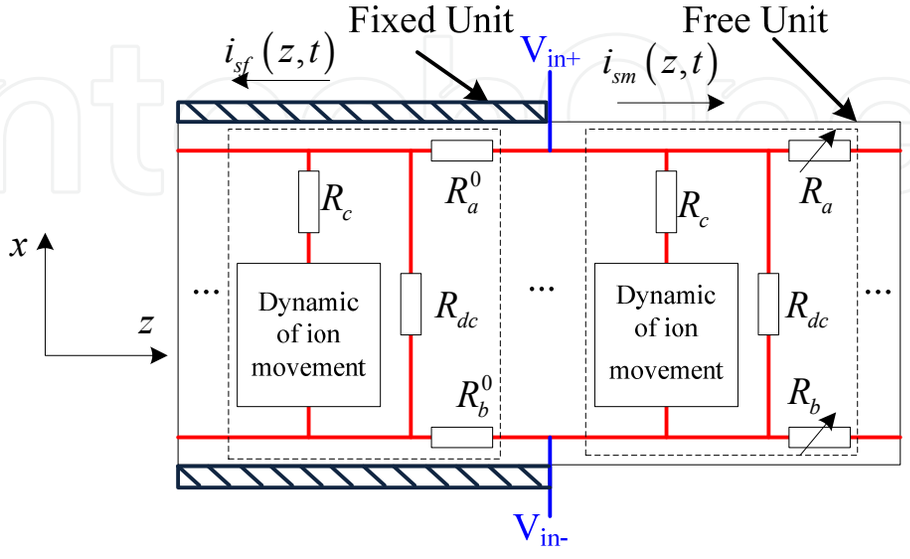

Figure 11. Equivalent circuit of an IPMC actuator

for moving. The actuator is then represented by the equivalent circuit in which affecting factors are defined as follows:

- R_a^0 , R_b^0 : the fixed surface resistances at both sides of the clamped part.
- R_a , R_b : the variable surface resistances at both sides of the movable part.
- $i_{sf}(z,t)$: the surface current of the movable part.
- $i_{sm}(z,t)$: the surface current of the movable part.

The analysis of self – sensing behavior deals with the following assumptions:

- The properties of the material are uniform. Consequently, surface resistances on both sides of the clamped part are equal:

$$R_a^0 = R_b^0 \tag{31}$$

- The variation of surface resistances is proportional to the unit bending displacement (the bending behavior corresponding to a unit length along the z axis). Given the unit bending displacement $\psi(z,t)$, the surface resistances on the movable part are calculated as follows:

$$\begin{cases} R_a(z,t) = \beta_a \psi(z,t) + R_a^0 \\ R_b(z,t) = \beta_b \psi(z,t) + R_b^0 \end{cases} \tag{32}$$

  where, and β_a, β_b are coupling constants to be determined by experiment.

- The neutral axis of the resistance variation is the center line of the IPMC along the z axis. This assumption allows one to treat β_a, β_b at same value:

$$\beta_a = -\beta_b = \beta \tag{33}$$

With the above assumption, the self – sensing ability of IPMC is discussed as follows. Define:

$$\begin{cases} \Delta R_a(z,t) = \beta_a \psi(z,t) \\ \Delta R_b(z,t) = \beta_b \psi(z,t) \end{cases} \tag{34}$$

Employing equation (33), the variant of surface resistance in equation (34) is rewritten as:

$$\Delta R_a(z,t) = -\Delta R_b(z,t) = \beta \psi(z,t) \tag{35}$$

A simplified circuit for the self – sensing actuator is carried out (figure 12)

Based on the equation (35), the following statements hold:

$$Z_F = Z_M = Z_{eq} \tag{36}$$

$$i_{sf}(z,t) = i_{sm}(z,t) = i_s(z,t) \tag{37}$$

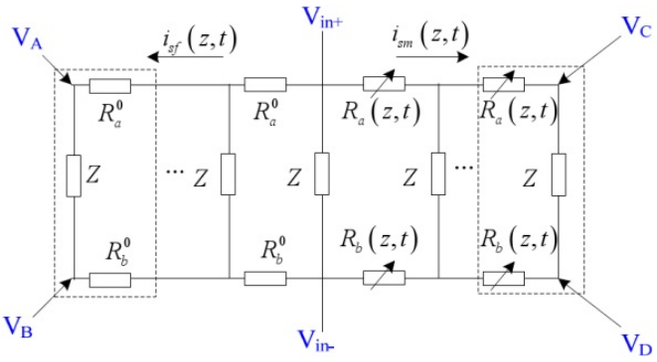

a) Specified circuit of an IPMC actuator

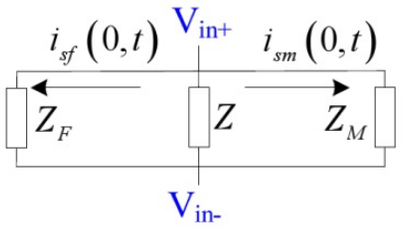

b) Equivalent impedance model

Figure 12. Simplified equivalent circuit of an IPMC actuator

where, Z_F, Z_M are equivalent impedance of fix part and movable part, respectively. The voltage signal at 4 points *A, B, C,* and *D* are in the forms:

$$V_A(t) = V_{in+}(t) - \int_0^{L/2} R_a^0 i_s(\tau,t)\,d\tau \tag{38}$$

$$V_B(t) = V_{in-}(t) + \int_0^{L/2} R_b^0 i_{sf}(\tau,t)\,d\tau \tag{39}$$

$$V_C(t) = V_{in+}(t) - \int_0^{L/2} R_a(\tau,t)\, i_{sm}(\tau,t)\,d\tau \tag{40}$$

$$V_D(t) = V_{in-}(t) + \int_0^{L/2} R_b(\tau,t)\, i_{sm}(\tau,t)\,d\tau \tag{41}$$

The following analyses are carried out:

$$\begin{aligned} V_{AC}(t) &= V_A(t) - V_C(t) = \int_0^{L/2} R_a(\tau,t) i_s(\tau,t)\,d\tau - \int_0^{L/2} R_a^0 i_s(\tau,t)\,d\tau \\ &= \int_0^{L/2} \left(R_a^0 + \Delta R_a(\tau,t)\right) i_s(\tau,t)\,d\tau - \int_0^{L/2} R_a^0 i_s(\tau,t)\,d\tau \\ &= \int_0^{L/2} \Delta R_a(\tau,t)\, i_s(\tau,t)\,d\tau \\ &= \beta \int_0^{L/2} \psi(\tau,t)\, i_s(\tau,t)\,d\tau \end{aligned} \tag{42}$$

Denote $V_{in+A}(t) = V_{in+}(t) - V_A(t)$, the derivatives of equation (38) and equation (42) give:

$$i_s(z,t) = \frac{1}{R_a^0}\frac{\partial V_{in+A}(t)}{\partial z} \tag{43}$$

$$\psi(z,t) = \frac{1}{\beta i_s(z,t)}\frac{\partial V_{AC}(t)}{\partial z} \tag{44}$$

$$\psi(z,t) = \frac{R_a^0}{\beta}\frac{\frac{\partial V_{AC}(t)}{\partial z}}{\frac{\partial V_{in+A}(t)}{\partial z}} \tag{45}$$

Note that R_a^0 is a constant. Equations (43), (44) and (45) imply that if one can observe the change of voltage signal along the length of IPMC actuator, the unit bending displacement can be obtained accurately. Consequently, the tip displacement of the IPMC can be obtained as follows:

$$d(t) = \int_0^{\frac{L}{2}} \psi(z,t) dz \tag{46}$$

In practice, the bending curvature can be estimated by using the feedback voltage signals at several points along the z axis. The following section presents the bending estimation of IPMC actuator using four points feedback configuration.

5.2. Experimental results for self sensing of an IPMC actuator

The self – sensing test rig using an IPMC actuator is shown in figure 13. Here, the actuator is a sheet of IPMC clamped by two plastic plates to which electrodes (V_{in+}, V_{in-}, A, B, C, and D) are attached and also contacted with two sides of the IPMC. The IPMC sheet in size of 30 x 6 x 0.2 mm manufactured by Environmental Robots Inc. can operate in both wet and dry environments. A processing system is built on a personal computer (Intel ® CoreTM2 Duo 1.8 GHz) within Simulink environment combined with Real-time Windows Target Toolbox of MATLAB. Two multi-function data acquisition Advantech cards, A/D 1711 and D/A 1720, are installed on PCI slots of the PC to perform the peripheral buses. In addition, a CCD laser displacement sensor, LK-081, from Keyence Corp. is installed on the rig base to measure the IPMC tip displacement.

Employing the technique described in section 5.1, the voltage signals at four points A, B, C, D are collected. In ideal case when the assumption in equations (31), (32), and (33) hold, the estimation can be done with only two feedback voltage signals at A and C. However, for more accurate result, the two more voltage signals at B and D are obtained. Since this implementation uses only four feedback signals, the equation (45) is rewritten as:

$$\psi(z,t) = \frac{R_a^0}{2\beta}\left(\frac{V_{AC}(t)}{V_{in+A}(t)} + \frac{V_{BD}(t)}{V_{in-}(t) - V_B(t)}\right) \tag{47}$$

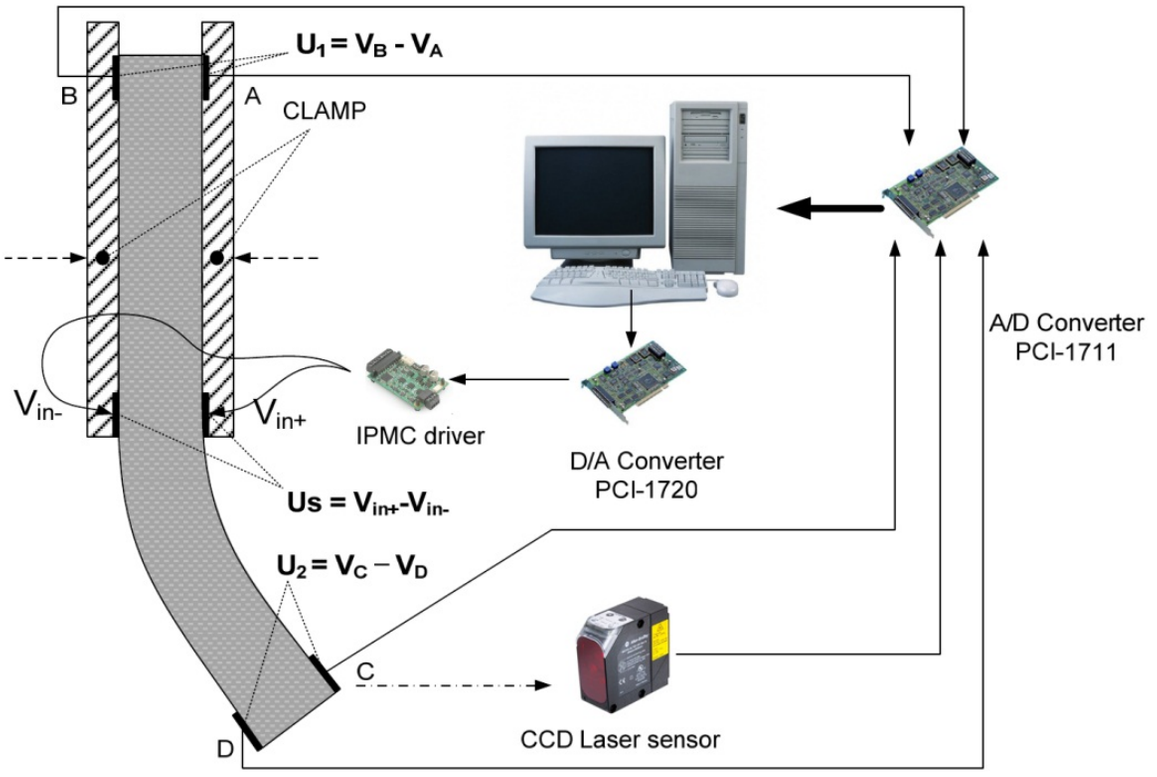

a) Configuration of IPMC in self – sensing application

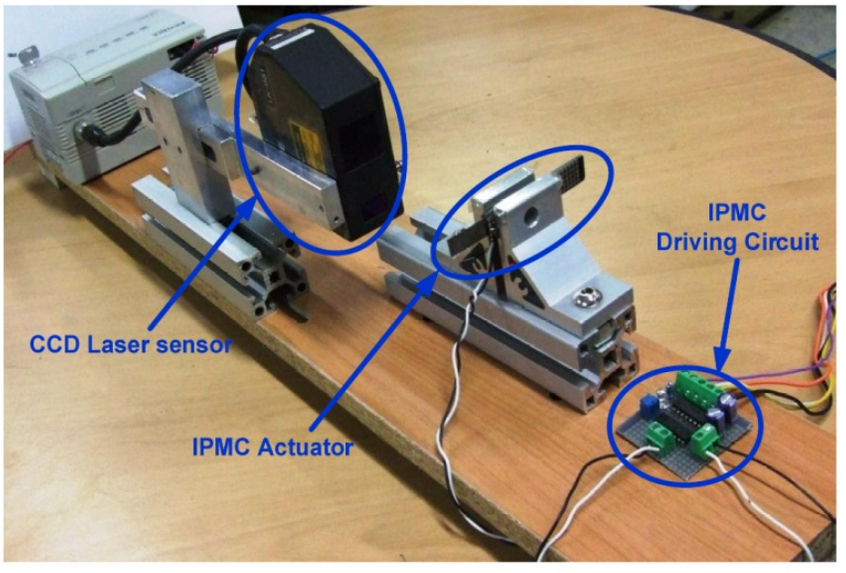

b) Experimental self – sensing IPMC actuator

Figure 13. Configuration of IPMC in self – sensing application

By applying equations (46) and (47), the self sensing has been carried out corresponding to four cases: 2V, 4V, 4.5V and 5V driving square input voltages signal, 0.05 Hz in frequency. Consequently, the experimental results are then shown in figure 14. Experimental results prove that the developed self – sensing technique has the ability to measure the bending behavior of the IPMC actuator. In order to increase the accuracy of the self sensing

performance, one can increase the number of captured voltage signals. However, the accuracy requirements depend on the practical application.

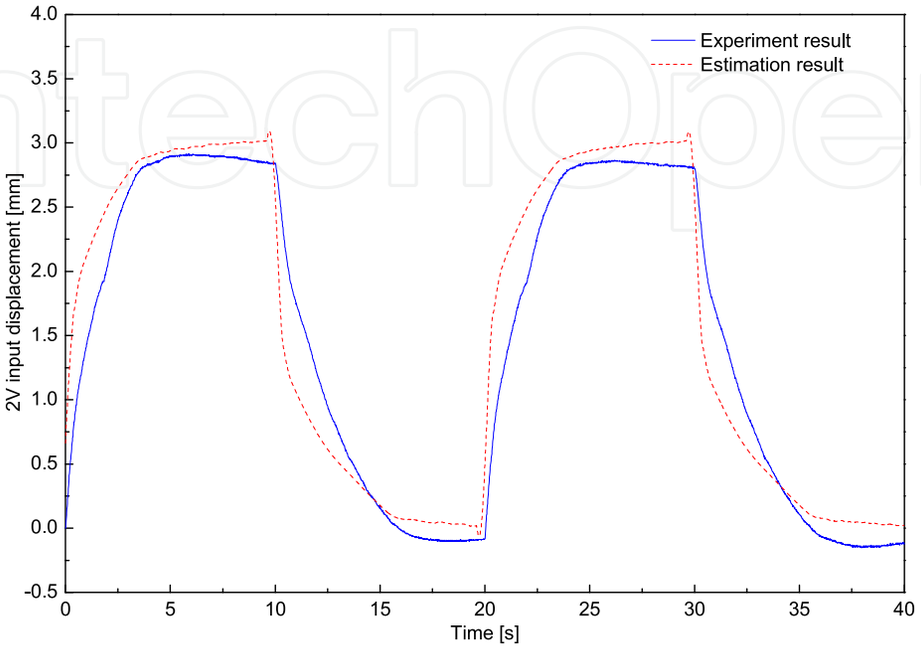

a) Estimation result – 2V square input signal

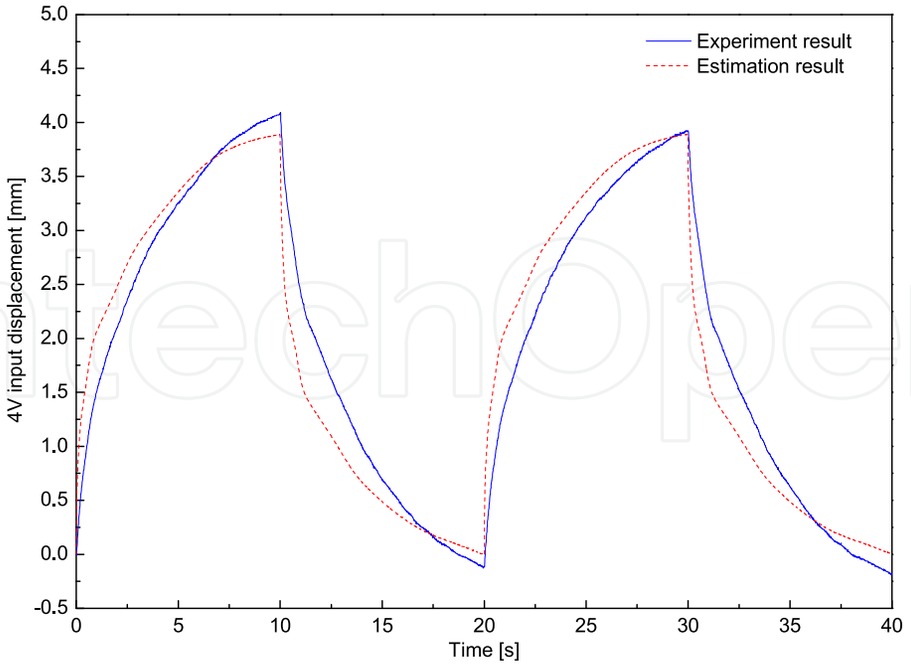

b) Estimation result – 4V square input signal

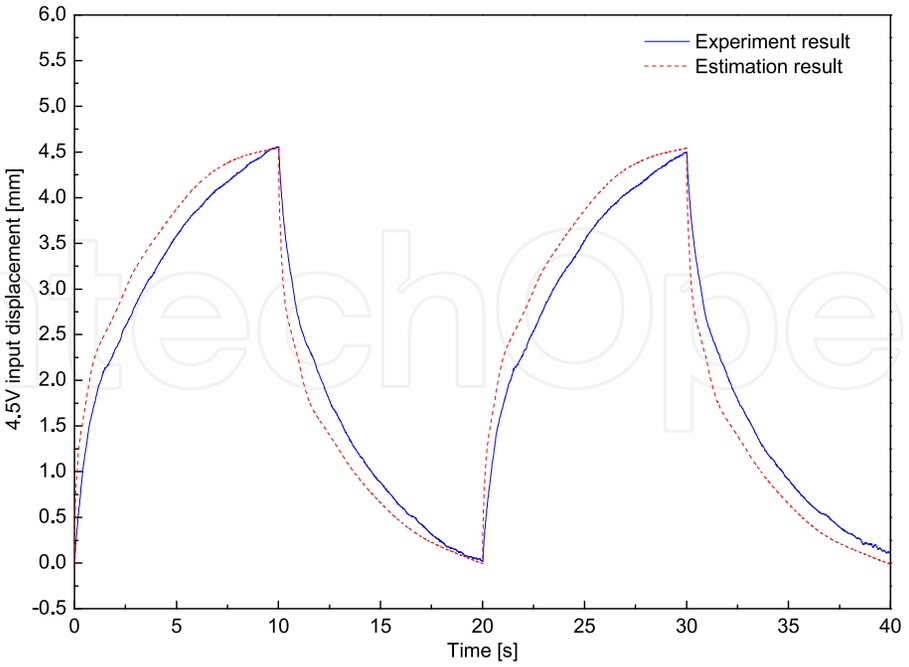

c) Estimation result – 4.5V square input signal

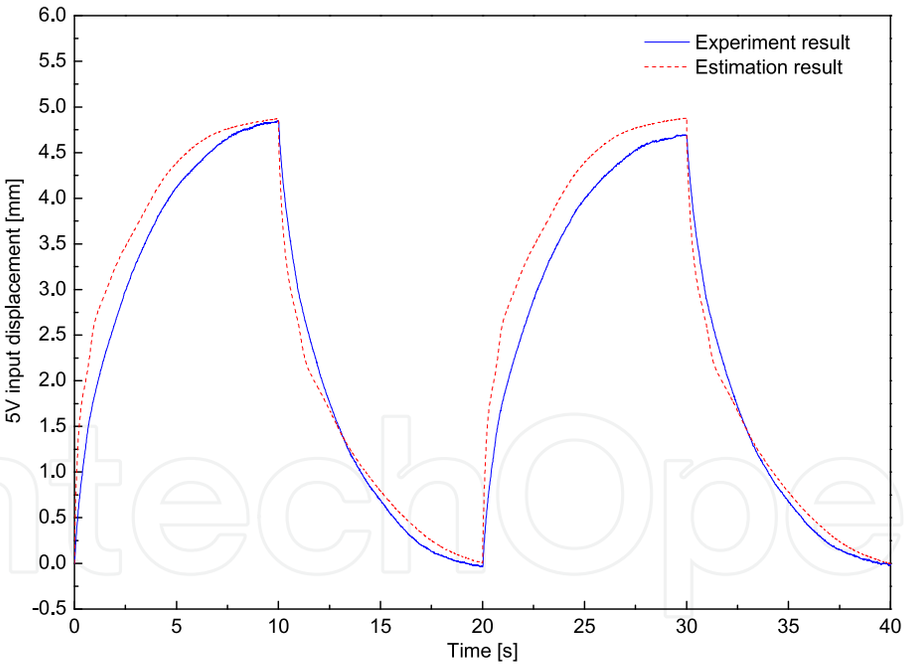

d) Estimation result – 5V square input signal

Figure 14. Self - sensing behavior of an IPMC actuator

6. Conclusion

This chapter gives a physical view in modeling the IPMC actuator and its self – sensing ability. The modeling technique provides a powerful tool to investigate the characteristic of

IPMC actuator via incorporation of physical induced stress model and visual ANSYS environment. The self – sensing model gives a powerful methodology to measure the displacement of IPMC actuator. This is a great advantage for biomedical, biomimetic, micro or mobile robotic applications where external sensing systems are usually unavailable.

Author details

Ahn Kyoung Kwan*
School of Mechanical and Automotive Engineering, University of Ulsan, Korea

Doan Ngoc Chi Nam
Graduate School of Mechanical and Automotive Engineering, University of Ulsan, Korea

Acknowledgement

This work was supported by the Korea Science and Engineering Foundation (KOSEF) grant funded by the Korea government (MEST) (No. 2009-0080924)

7. References

[1] Ba-Cohen Y. (2001) Electro-Active polymer (EAP) actuators as artificial muscles - Reality, potential, and challenges, Spie press .

[2] Abadi S., Dehghani A., Nelson E.A. (2008) A soft sensing method for monitoring ambulatory activities of patients with venous ulceration, Proc. of the 4th IET Int. Conf. on Adv. in Medical, Sig. and Inf. Processing, MEDSIP. pp.1 – 4.

[3] Paola B., Fortuna L., Giannone P., Graziani S., Strazzeri S. (2008) IPMCs as Vibration Sensors, Proc. of IEEE Int. Instrumentation and Measurement Tech. Conf. pp.2065 – 2069.

[4] Bonomo C., Fortuna L., Giannone P., Graziani S. (2004) A sensor-actuator integrated system based on IPMCs [ionic polymer metal composites], Sensors, Proc. of IEEE conf. pp. 489 – 492.

[5] Fang B.K., Lin C.-C.K., Ju M.-S. (2010) Development of Sensing/Actuating Ionic Polymer Metal-Composite (IPMC) for Active Guide-Wire System, Sensors & Actuators: A. Physical, v 158, pp. 1-9.

[6] Chen Z., Kwon K.Y., Xiaobo T. (2008) Integrated IPMC/PVDF sensory actuator and its validation in feedback control, Sen. and Act. A: Physical 144(2), pp. 231-241.

[7] Yamakita M., Kamamichi N., Kozuki T., Asaka K., Zhi-Wei L. (2005) A snake-like swimming robot using IPMC actuator and verification of doping effect, Proc. of IEEE/RSJ Int. Conf. pp.2035 – 2040

[8] Tung N.T., Khanh N.V., Youngtai Y., Goo N.S. (2006) A Novel Polymeric Micropump based on a Multilayered Ionic Polymer-Metal Composite, Proc. of IECON - 32nd Annual Conference, pp.4888 – 4893.

* Corresponding Author

[9] Yamakita M., Kamamichi N., Kozuki T., Asaka K., Zhi-Wei L. (2005) Control of Biped Walking Robot with IPMC Linear Actuator, Proc. of IEEE/ASME International Conference, Sep. pp.48 – 53.
[10] Guo S., Shi L., Asaka K. (2008) IPMC actuator-sensor based a biomimetic underwater microrobot with 8 Legs, Proc. of ICAL. IEEE International Conference, Sep. 2008, pp.2495 – 2500.
[11] Punning A., Kruusmaa M. and Aabloo A. (2009) Surface resistance experiments with IPMC sensors and actuators Sen. and Act. A: Physical 133(1). Pp. 200-209.
[12] Punning A., Kruusmaa M. and Aabloo A. (2007) A self-sensing ion conducting polymer metal composite (IPMC) actuator Sen. and Act. A: Physical 136(2). Pp. 656-664.
[13] Nemat-Nasser S. and Li J. (2000) Electromechanical response of ionic polymer-metal composites, Journal of Applied Physics, 87 (7), pp. 3321–3331.
[14] Farinholt K. M. (2005) Modeling and characterization of ionic polymer transducers for sensing and actuation, Ph.D. dissertation, Virginia Polytechnic Institute and State University.
[15] Chen Z. and Tan X. (2008) A control-oriented and physics-based model for ionic polymer –metal composite actuators, IEEE/ASME Trans. Mechatronics. 13, pp. 519–529.
[16] Chen Z., Hedgepeth D. R. and Tan X. (2009) A nonlinear, control-oriented model for ionic polymer–metal composite actuators, Smart Mater. Struct. 18055008 (9pp).
[17] Nemat-Nasser S. (2002) Micromechanics of Actuation of Ionic Polymer-metal Composites, Journal of Applied Physics, 92 (5) (21pp).
[18] http://www.ansys.com/Support/Documentation